Temperature dependence of bulk and interface contributions to the magnetic damping of Permalloy thin films

Verena Ney,[1] Kilian Lenz,[2] Fabian Ganss,[2] René Hübner,[2] Jürgen Lindner,[2] and Andreas Ney[1,*]
[1]*Johannes Kepler University Linz, Institute for Semiconductor and Solid State Physics, Altenberger Str. 69, 4040 Linz, Austria*
[2]*Helmholtz-Zentrum Dresden-Rossendorf, Institute of Ion Beam Physics and Materials Research, Bautzner Landstr. 400, 01328 Dresden, Germany*

(Received 13 November 2025; accepted 3 February 2026; published 23 February 2026)

The magnetic damping of $Ni_{80}Fe_{20}$ [Permalloy (Py)] thin films is studied via temperature- and frequency-dependent ferromagnetic resonance (FMR) as a function of the Py layer thickness for two different thickness series, Al/Py/sapphire and Al/Py/Al/sapphire, respectively. Additional magnetic and structural characterization is done by superconducting quantum interference device magnetometry as well as x-ray reflectivity and transmission electron microscopy. The frequency dependence of the FMR linewidth allows us to separate the Gilbert-like contributions from non-Gilbert-like ones like two-magnon scattering (TMS) processes. The thickness dependence allows us to separate the derived magnetic parameters such as saturation magnetization M_s, TMS contribution Γ, and Gilbert damping parameter α into their respective bulk and interfacial contributions. While the bulk contribution α^{bulk} monotonously decreases with temperature from 0.0061(1) down to 0.0054(1) for both samples series, the interfacial contribution $\alpha^{interface}$ shows a subsequent increase at low temperature. This is rather pronounced for the Al/Py/sapphire series, caused by a temperature-dependent TMS contribution. For the Al/Py/Al/sapphire series, the increase at low temperatures is much less pronounced, and a temperature-independent TMS contribution is only found for the thinnest sample due to a wavy Py film morphology. Correcting for the TMS contributions allows us to extract $\alpha^{bulk}(T)$ which reflects the intrinsic magnetic damping properties of sputtered Py thin films.

DOI: 10.1103/61vn-39dq

I. INTRODUCTION

The magnetization dynamics of a ferromagnet in an external magnetic field can be described by the well-known Landau-Lifshitz equation [1], which was later modified by Gilbert [2], who introduced a phenomenological damping parameter α. In this form, the relaxation is treated—in analogy to the situation of a viscous medium—via a term being proportional to the velocity of its motion. However, in this approach, contributions to the damping are neglected which alter the size of the magnetization. A Gilbert-like damping α gives rise to a linear increase of the linewidth in ferromagnetic resonance (FMR) experiments as a function of microwave frequency f_{MW}. While Gilbert damping is often referred to as homogeneous damping, Gilbert-like, i.e., linear-in-frequency, damping can already contain several other linear-in-frequency contributions, e.g., eddy current or radiative damping [3,4], which are unavoidably present. It has been discussed in detail in Ref. [5] that these can be considered small for thin ferromagnetic films below about 20 nm. Additional Gilbert-like contributions also arise in cases where spin pumping into adjacent capping or spacer layers is present [6]. If all these contributions are absent or can be considered negligible, the underlying mechanism for the remaining intrinsic part of Gilbert damping is ultimately based on the dissipation of energy via spin-orbit coupling into the lattice [7]. Following modeling introduced by Kambersky [8,9], two different mechanisms can contribute: On the one hand, there is an interband scattering mechanism which leads to a resistivitylike behavior of α with temperature, i.e., increased electronic scattering (= higher resistivity) leads to an increased α [8]. On the other hand, there is the intraband scattering mechanism associated with the breathing Fermi surface model, which leads to a conductivitylike behavior of α, i.e., α increases upon reduced electronic scattering [9]. If both mechanisms are present at the same time, this leads to higher Gilbert damping at very low and at elevated temperatures and eventually a local minimum at intermediate temperatures, depending on the respective magnitude of the two contributions. Both contributions can also be modeled using a single scattering rate leading to the contributions from the breathing Fermi surface (due to intraband scattering) for the conductivitylike contributions and the bubbling Fermi surface (due to interband scattering) for the resistivitylike contributions, respectively [10]. The temperature dependence $\alpha(T)$ of the Gilbert damping has experimentally been observed or verified in several metallic thin ferromagnetic films, see, e.g., Ref. [11] for a comprehensive discussion of the existing literature and experimental evidence for the presence of a conductivitylike contribution in epitaxial Fe.

Before intrinsic Gilbert(-like) damping can be studied experimentally, one must make sure that all non-Gilbert-like

*Contact author: andreas.ney@jku.at

contributions are absent. One relevant mechanism is given by two-magnon scattering (TMS) processes, which lead to a nonlinear frequency dependence of the FMR linewidth [12,13]. Such two-magnon processes can only be studied using broadband FMR because they lead to a characteristic nonlinear frequency dependence at lower frequencies, which saturates at higher $f_{\rm MW}$ [12] or even decreases [13]. For example, it was recently demonstrated for thin films of $Ni_{80}Fe_{20}$ [Permalloy (Py)] that oxidic cap layers induce two-magnon processes which are present only at low temperatures [14]. Another mechanism of activating TMS contributions to the overall magnetic damping are wavy interfaces which can be induced by the islandlike growth of Al spacer layers between Py and an oxidic substrate like sapphire which are essentially temperature independent [15]. While these TMS processes unavoidably contribute to the overall magnetic damping, they must be subtracted from the frequency dependence of the FMR linewidth to obtain the remaining intrinsic Gilbert damping parameter and its temperature dependence. A final step in the analysis of the Gilbert damping is its dependence on the thickness of the thin ferromagnetic film, which allows us to separate the bulk and interface contributions to the damping. Such a separation has been reported for Py thin films studied by temperature-dependent broadband FMR in Ref. [16]. However, in that work, the frequency range was limited to 15 GHz, which is below the frequency where TMS processes become evident; for Py, this is typically around 15–20 GHz, see Refs. [14,15]. Therefore, eventual TMS contributions might have been overlooked in Ref. [16], and the reported $\alpha(T)$ behavior may be different from the intrinsic one.

Here, we report on a systematic study of the temperature and frequency dependence of the FMR linewidth of two thickness series, Al/Py/sapphire and Al/Py/Al/sapphire, respectively. Al spacer layers between Py and sapphire have been reported to be beneficial for reducing the overall FMR linewidth; however, the thickness of the Al spacer layer must be below 3 nm to suppress unwanted TMS contributions [15]. For both sample series, only the thickness of the Py layer d has been varied from 3.4 nm up to 37.1 nm. It is the aim of this work to separate the magnetic properties of Py into their bulk and interface contributions and their respective temperature dependencies. Ideally, the interface contribution scales linearly with $1/d$, whereas the bulk contributes with a constant proportion. Via the frequency dependence of the FMR linewidth, the magnetic damping can be separated into Gilbert-like and non-Gilbert-like contributions, the former being linear in frequency, the latter being mostly TMS contributions for the Al/Py/sapphire sample series, which are nonlinear in frequency and only present at low temperatures. In the Al/Py/Al/sapphire sample series, the TMS contribution is only observed for the thinnest Py film and is temperature independent. It is attributed to a wavy microstructure of the Py film similar to the observations in Ref. [15]. Removing the interface and/or TMS contributions from the FMR linewidth, the remaining bulk contribution to the Gilbert-like damping $\alpha^{\rm bulk}$ can be considered the intrinsic properties of magnetron-sputtered Py thin films, and its temperature dependence is found to be exclusively resistivitylike, i.e., no increase of $\alpha^{\rm bulk}$ toward lower temperature is observed. Instead, $\alpha^{\rm bulk}(T)$ monotonously decreases from 0.0061(1) at 295 K down to 0.0054(1) at 10 K, being constant below 100 K. In contrast, conductivitylike Gilbert damping behavior is only observed in the interfacial contribution $\alpha^{\rm interface}(T)$.

II. EXPERIMENTAL DETAILS

The Al-capped (Al/Py/sapphire) and sandwiched (Al/Py/Al/sapphire) Py thin films were grown by magnetron sputtering at ambient temperature on epi-ready c-plane sapphire [Al_2O_3 (0001)] substrates in an ultrahigh vacuum system with a base pressure of 2×10^{-9} mbar. The working pressure was 4×10^{-3} mbar for both Al and Py using 10 sccm Ar and a sputter power of 20 W, respectively. The growth rates of 5.3 ± 0.2 nm/min for Py and Al were monitored using a quartz crystal microbalance (QCM). Throughout this work, the nominal thickness of the Al cap was set to 5 nm, and the nominal thickness of the Al spacer was set to 2 nm, which was found to be the optimum thickness [15]. The thickness of the Py layer was varied from nominally 5 nm up to 50 nm. The actual thickness was determined by x-ray reflectivity (XRR) and partially cross-checked using transmission electron microscopy (TEM), which yielded a thickness range from 3.4 to 37.1 nm for the Py layer. The structural characterization by XRR was done with a parallel beam of Cu K_α radiation (Rigaku SmartLab). XRR data were modeled using the SmartLab Studio II software from Rigaku; model stacks were systematically varied, and various slightly altered initial configurations were tested to assure the robustness of the resulting fit parameters.

Standard magnetic characterization was carried out using a superconducting quantum interference device (SQUID) magnetometer (Quantum Design, MPMS XL-5). The external magnetic field was applied in the film plane to record the easy-axis $M(H)$ curves of Py at room temperature. From these, the saturation magnetization $M_{\rm s}$ and coercive field $H_{\rm c}$ were determined. To record the very low $H_{\rm c}$ of Py, the superconducting magnet must be reset before the measurement, and magnetic fields larger than 10 mT must be avoided to limit the unwanted residual offset field to around 0.1 mT (so-called flux trapping, see Ref. [17]). As a consequence, $H_{\rm c}$ cannot be determined with an accuracy better than 0.1 mT, and for all samples under investigation, H_c remained below 0.2 mT [see inset of Fig. 1(b)]. Here, $M_{\rm s}$ is derived by linearly extrapolating the measured $m(H)$ behavior to zero field, see inset of Fig. 1(b), which leads to an uncertainty of the derived magnetic moment m of less than a percent. For conversion of $m(H)$ into $M(H)$, the sample volume is needed which is derived from the thickness of the Py as determined via XRR/TEM, resulting in an uncertainty of typically 2%. The sample area was determined via an optical microscope, which causes an additional uncertainty of 1%. Thus, the resulting accuracy of the $M_{\rm s}$ values derived by SQUID is at best 3%.

The cross-sectional TEM specimen preparation was done by *in situ* liftout using a Helios 5 CX focused ion beam (FIB) device (Thermo Fisher). To protect the sample surface, a carbon cap layer was deposited beginning with electron-beam-assisted and subsequently followed by Ga-FIB-assisted precursor decomposition. Afterward, the TEM lamella was prepared using a 30 keV Ga-FIB with adapted

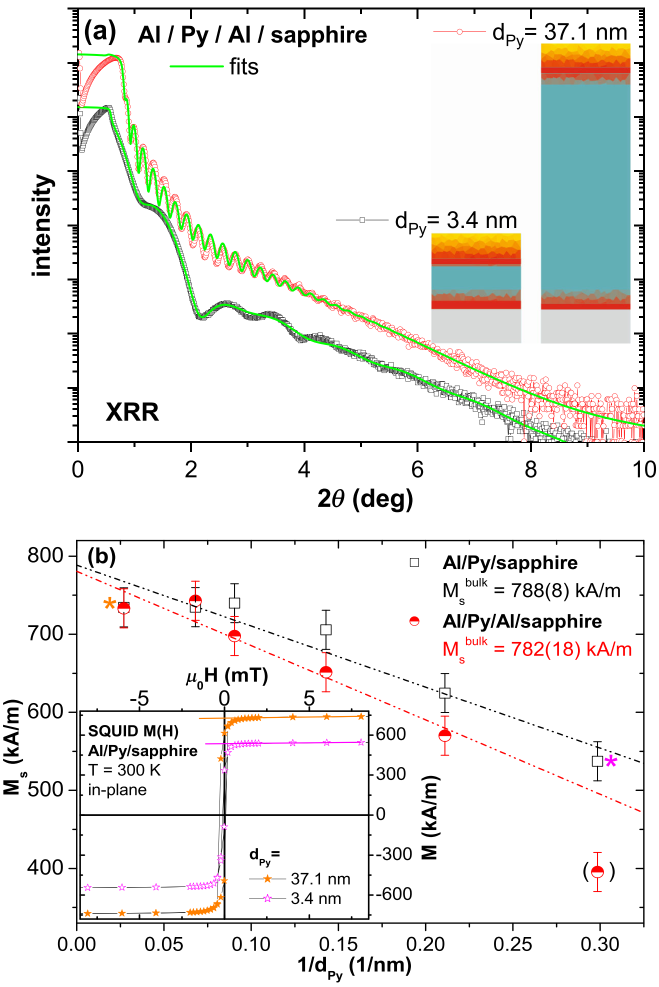

FIG. 1. (a) XRR measurements for the 37.1- and 3.4-nm-thick Al/Py/Al/sapphire sample together with a fit using the sketched stack. (b) SQUID $M(H)$ measurements in in-plane geometry at 300 K for all samples under investigation. The inset exemplarily shows the thinnest (open stars) and thickest (full stars) samples without a spacer. A linear fit to the M_s vs $1/d$ data allows us to extract the bulk value of M_s of Py; the thinnest sample with an Al spacer was excluded from the analysis, see text.

currents. Its transfer to a three-post copper liftout grid (Omniprobe) was done with an EasyLift EX nanomanipulator (Thermo Fisher). To minimize sidewall damage, Ga ions with only 5 keV energy were used for final thinning of the TEM lamella to electron transparency. Prior to TEM analysis, the specimen mounted in a high-visibility low-background holder was placed for 10 s into a Model 1020 Plasma Cleaner (Fischione) to remove potential contamination. High-angle annular dark-field scanning transmission electron microscopy (HAADF-STEM) imaging and spectrum imaging analysis based on energy-dispersive x-ray spectroscopy (EDXS) were performed at 200 kV with a Talos F200X microscope equipped with a Super-X EDX detector system (FEI). Line-by-line intensities of the EDXS elemental distribution maps were computed to obtain element intensity profiles across the sample stack, as described in greater detail in Ref. [15].

Temperature-dependent broadband FMR measurements were carried out using the NanOsc Cryo-FMR40 setup with a microwave frequency f_{MW} in the range of 2–40 GHz. The sample was placed on a coplanar waveguide assembly with a fixed polar angle of $\theta_{\mathrm{H}} = 90^\circ$ (in-plane), and the transmitted microwave power was detected by a diode. The static external magnetic field $\mu_0 H_{\mathrm{ext}}$ as well as the temperature control is provided by a Quantum Design PPMS system. The FMR spectra are recorded at a fixed microwave frequency as a function of the external field, which is changed step by step; the step size is chosen such that at least 12 field points are recorded across the given linewidth. A pair of Helmholtz coils supplies an external alternating magnetic field for lock-in detection, and the field modulation amplitude is kept below the step size of the external field and thus well below the actual linewidth. Therefore, the resonance line is not distorted by undersampling and remains purely of Lorentzian shape, see FMR spectra, Fig. 2(a). The individual FMR spectra are fitted with a Lorentzian derivative, which allows us to extract the resonance field H_{res} as well as the FMR linewidth ΔH. Note that, throughout this work, ΔH, which refers to the full width at half maximum, is mostly converted to the peak-to-peak linewidth ΔH_{pp}; the relation is $\Delta H_{\mathrm{pp}} = \Delta H/\sqrt{3}$.

In a typical FMR experiment, the so-called Kittel plots, i.e., f_{MW} as a function of $\mu_0 H_{\mathrm{res}}$, are collected at selected temperatures. These datasets can be fitted with the following resonance equation for $\theta_{\mathrm{H}} = 90^\circ$ (in-plane):

$$\left(\frac{2\pi f_{\mathrm{MW}}}{\gamma}\right)^2 = \left(\mu_0 H_{\mathrm{res}} + \mu_0 M_{\mathrm{eff}} + \frac{2K_{2\parallel}}{M_s}\right) \times \left(\mu_0 H_{\mathrm{res}} + \frac{2K_{2\parallel}}{M_s}\right). \quad (1)$$

Here, γ is the gyromagnetic ratio, which is related to the g factor by $\gamma = g\mu_{\mathrm{B}}/\hbar$, where μ_{B} is the Bohr magneton, and $\hbar$ is the reduced Planck constant. Also, H_{res} denotes the resonance field extracted from the individual FMR spectra, $K_{2\parallel}$ is the in-plane uniaxial anisotropy, and $\mu_0 M_{\mathrm{eff}} = \mu_0 M_s - 2K_{2\perp}/M_s$ is the effective magnetization, where $K_{2\perp}$ is the out-of-plane uniaxial anisotropy. In the ideal case of Py where no crystalline anisotropy should be present, $K_{2\parallel}$ and $K_{2\perp}$ should be zero, and thus, $\mu_0 M_{\mathrm{eff}}$ should be equal to $\mu_0 M_s$; this has already been verified for the 14.7-nm-thick samples of the present series in Ref. [15].

A second set of data, which is more central to the present study, can be derived from the frequency dependence of the FMR linewidth ΔH_{pp}. These data can be fitted using the following equation:

$$\Delta H_{\mathrm{pp}} = \frac{4\pi\alpha}{\sqrt{3}\gamma} f_{\mathrm{MW}} + \delta\mu_0 K_{2\parallel} \left|\frac{\partial H_{\mathrm{res}}}{\partial(\mu_0 K_{2\parallel})}\right| + \Delta H_{\mathrm{TMS}}. \quad (2)$$

Here, α is the Gilbert damping parameter. Deviations from the linear behavior of $\Delta H(f_{\mathrm{MW}})$ indicate additional contributions to the FMR linewidth such as TMS processes (ΔH_{TMS}), which typically exhibit a nonlinear frequency dependence at lower frequencies, which becomes almost constant at higher f_{MW} [12] or even decreases [13], which leads to a characteristic kink in $\Delta H(f_{\mathrm{MW}})$ around 15–20 GHz. Throughout this study, it was sufficient to model the TMS processes with a simplified Mills model with the explicit correlation function of the scattering centers, i.e., magnetic roughness (of any kind) is not explicitly considered; instead, a single parameter Γ_H is used

$$\Delta H_{\mathrm{TMS}} = \Gamma_H \arcsin\sqrt{\left(\frac{[\omega^2 + (\omega_0/2)^2]^{1/2} - \omega_0/2}{[\omega^2 + (\omega_0/2)^2]^{1/2} + \omega_0/2}\right)} \quad (3)$$

Here, $\omega_0 = -\gamma 4\pi M_{\mathrm{eff}}$ and $2\pi\omega = f_{\mathrm{MW}}$, and the fieldlike parameter Γ_H can be converted into a scattering rate Γ by multiplying with the gyromagnetic ratio. This model is sufficient to satisfyingly fit the measured $\Delta H_{\mathrm{pp}}(f)$ dependencies, see also Ref. [15] for the 14.7 nm sample pair of this study. An additional FMR linewidth broadening due to sample inhomogeneity is factored in by considering a spread (variation over the sample) of the in-plane uniaxial anisotropy ($\delta K_{2\parallel}$). Note, that the mosaicity $\delta\mu_0 M_{\mathrm{eff}}$ can also contribute to the FMR linewidth, but throughout this work, no evidence for this contribution has been found. It is common that mosaicity contributions are often not considered separately, see, e.g., Refs. [11,14,16]; instead, a simplified version of Eq. (2) is used

$$\Delta H = \Delta H_0 + \frac{4\pi\alpha}{\gamma} f_{\mathrm{MW}}. \quad (4)$$

Here, the Gilbert damping parameter α is nominally identical to Eq. (2), and the inhomogeneous contribution to the FMR linewidth is put into a frequency-independent offset ΔH_0. Since H_{TMS} is not included, there is the danger that, for slight deviations from the linear dependence of $\Delta H(f_{\mathrm{MW}})$, the TMS contribution is overlooked, especially if the f_{MW} range is limited to below 15–20 GHz and only Eq. (4) is used for fitting, which artificially increases the extracted values for α and/or ΔH_0; this will become more evident during the discussion of the data further below.

To separate bulk and interface contributions of magnetic parameters such as the damping constant α, one can follow a simple model assumption which is very common in experimental works like Refs. [16,18] and confirmed by theory [19]

$$\alpha = \alpha^{\mathrm{bulk}} + \frac{\alpha^{\mathrm{interface}}}{d}. \quad (5)$$

The thickness series of the Py films contains samples with nominally 5, 7, 10, 15, 20, and 50 nm, which correspond to actual thicknesses of 3.4, 4.7, 7.0, 11.1, 14.7, and 37.1 nm (±0.5 nm), as determined by XRR for all samples, which was confirmed by TEM except for the nominally 10- and 15-nm-thick samples. This thickness series allows us to separate all extracted magnetic parameters into their formal bulk and interface contributions by analyzing them when plotted against $1/d$. The range of Py film thicknesses is limited by the detection limit of the Cryo-FMR for thinner samples and by the penetration depth of the microwave for thicker samples, the latter leading to non-Lorentzian FMR line shapes for thicker Py films. Note that the discrepancy between the nominal thickness as determined by the growth rate via QCM and the actual one is systematic and not present for the nonmagnetic Al cap/spacer layers (and others, not shown) despite that the proper values were used for density and tooling factor for the QCM. We tentatively ascribe that to a magnetostatic interaction between the magnet assembly of the magnetron used for sputtering and the deposited ferromagnetic film. It is noteworthy that extracted bulk and interface contributions differ significantly if the nominal thicknesses are used.

III. EXPERIMENTAL RESULTS

A. Structural and basic magnetic characterization

Figure 1(a) shows the XRR measurements of the 3.4-nm-thick (squares) and 37.1-nm-thick (circles) Py films of the Al/Py/Al/sapphire series together with the respective fits. The fit parameters are visualized by the two schematic stacks; more details about this visualization can be found in Ref. [15], where an identical procedure has already been used. Most importantly, the interface between Py and Al cap and spacer are not ideal and must be modeled not only by roughness but also by an interfacial layer with a density which was allowed to vary between those of Al and Py. This is necessary to account for some degree of waviness, which was already discussed for the 14.7 nm film in Ref. [15] and will be evidenced more directly by TEM further below, where it is especially pronounced for the 3.4 nm film, see Fig. 4(b). The relatively strong suppression of the XRR oscillations for the 3.4-nm-thick film together with the somewhat limited quality of the fit already indicates that the thinnest Al/Py/Al/sapphire sample has the lowest structural perfection of the entire series. It should be noted that, in general, the quality of the XRR data and respective fits of the Al/Py/sapphire sample series are higher (not shown) due to the well-defined interface between Py and sapphire, see Ref. [15] for the 14.7 nm film. Therefore, the actual thickness was derived from this series, and it is assumed that the respective thickness of the sample from the Al/Py/Al/sapphire series, which was always grown right after the one from the Al/Py/sapphire series, is identical; this avoids an additional uncertainty due to the Py/Al interfacial layer, where it is difficult to assess which fraction of the interfacial layer must be counted toward the effective Py thickness and which contributes to the Al spacer layer.

Figure 1(b) summarizes the findings of the standard magnetic characterization using SQUID magnetometry. The inset exemplarily shows two $M(H)$ curves recorded at 300 K in in-plane orientation of the thickest (full stars) and thinnest (open stars) Al/Py/sapphire samples, respectively. It is clearly visible that M_s of the thinnest sample is reduced compared with the thickest one. Plotting M_s of the Al/Py/sapphire (open squares) and Al/Py/Al/sapphire (half full circles) series vs inverse Py thickness d_{Py}, a rather linear behavior is observed for both series except the thinnest Al/Py/Al/sapphire sample, which is excluded from further analysis (see below). Both series consistently yield a bulk contribution to M_s of 788(8) and 782(18) kA/m, which are both within experimental accuracy, in agreement with the established value for Py of 790 kA/m. The interfacial contribution is a reduction of M_s, presumably due to slight intermixing with the adjacent Al layer(s), and thus, it is slightly more pronounced for the Al/Py/Al/sapphire series. This slight reduction has already been discussed on the basis of the 14.7-nm-thick sample pair in Ref. [15]. In summary, both sample series consist of structurally smooth and well-defined Py layers with the expected basic properties as far as a characterization using XRR and SQUID is concerned.

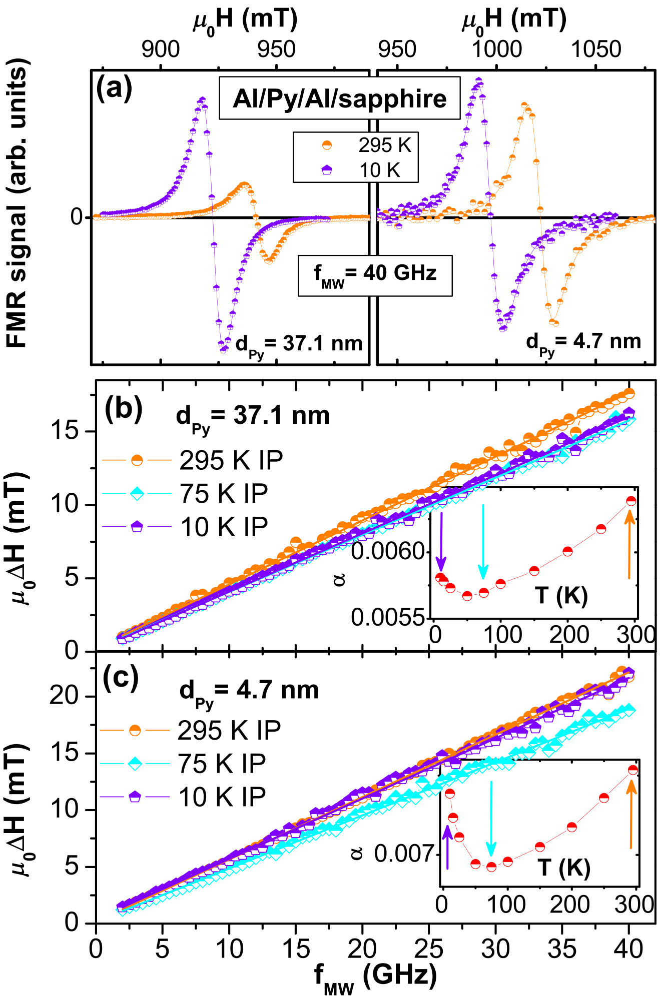

FIG. 2. (a) FMR spectra at 40 GHz for 295 K (orange circles) and 10 K (violet pentagons) of the thickest (left) and second-thinnest (right) Al/Py/Al/sapphire samples with Py thicknesses of 37.1 nm (left) and 4.7 nm (right) together with the respective fits using a Lorentzian derivative (lines). Full frequency dependence of the fitted linewidth $\Delta H(f)$ of the respective (b) thick and (c) thin samples of (a) for selected temperatures as measured by Cryo-FMR. The insets in (b) and (c) show the full temperature dependence $\alpha(T)$ for the thickest and second-thinnest samples, respectively.

Only the thinnest Al/Py/Al/sapphire sample is structurally less ideal in that regard.

B. Magnetic damping

Figure 2 exemplarily summarizes the characterization of the second-thinnest and thickest samples of the Al/Py/Al/sapphire series using Cryo-FMR; the thinnest sample, which was already excluded from the SQUID analysis will be discussed separately further below. Figure 2(a) compares the FMR spectra recorded at 295 K (orange circles) and 10 K (violet pentagons) for the thickest (left) and second-thinnest (right) samples at 40 GHz, i.e., at the experimental conditions with the lowest signal-to-noise ratio. In all cases, the line shape is a clear Lorentzian derivative with the onset of a slight asymmetry for the thickest sample at low temperatures due to the finite microwave penetration depth; the symbols correspond to the experimental data, while lines are the respective fits using a complex Lorentzian derivative as implemented in the NanOsc software of the Cryo-FMR. From the fits, both H_{res} and ΔH are extracted; in the following, we will exclusively focus on the FMR linewidth since the magnetic parameters derived by the Kittel fit according to Eq. (1) only yield M_{eff} consistent with the findings of the SQUID [20], a negligible in-plane uniaxial anisotropy $K_{2\parallel}$, and a comparably slight reduction of g with temperature, as already discussed for the 14.7 nm pair of samples in Ref. [15].

Figures 2(b) and 2(c) show the frequency dependence of the FMR linewidth $\Delta H(f_{\mathrm{MW}})$ at 295 K, 75 K (cyan diamonds), and 10 K of the 37.1 and 4.7 nm samples, respectively. A linear behavior of all $\Delta H(f_{\mathrm{MW}})$ curves is observed demonstrating purely Gilbert-like behavior described by Eqs. (2) and (4), i.e., the absence of any significant contribution from ΔH_{TMS}. From the slope, the temperature dependence of the Gilbert damping parameter $\alpha(T)$ can be derived as shown in the insets of Figs. 2(b) and 2(c); arrows indicate the data points derived from the displayed data; and typical error bars are smaller than the symbol size. For both samples, a decrease of α with temperature is observed down to 75 K followed by an increase of α at low temperatures, which is more pronounced in the 4.7-nm-thick sample (c); also, the overall $\alpha(T)$ is larger for the thinner sample.

So far, the 3.4 nm Al/Py/Al/sapphire sample has been excluded from the discussion. Figure 3(a) shows the frequency dependence of the peak-to-peak linewidth $\Delta H_{\mathrm{pp}}(f_{\mathrm{MW}})$ for the thinnest sample at 295 K. A slight curvature of the data is visible; therefore, the FMR linewidth must be modeled using Eq. (2), i.e., including a finite ΔH_{TMS} contribution; the best fit in this case yields a two-magnon contribution of $\Gamma = 0.55\,\mathrm{GHz}$, a Gilbert damping $\alpha = 0.0092$, and a negligible mosaicity contribution. For comparison, a fit using Eq. (4) is shown (dashed gray line), where the TMS contribution is neglected. This fit yields $\alpha = 0.0109$, thus an apparently increased Gilbert damping; however, deviations between fit and experimental data are clearly visible. This comparative analysis using either equation has been performed for all temperatures, and Fig. 3(b) summarizes the findings. The fit using Eq. (4), i.e., not removing the TMS contribution to the linewidth, yields a systematically higher $\alpha(T)$, as shown in the inset (gray triangles). Likewise, the inhomogeneous contribution ΔH_0 is finite, between 1 and 1.5 mT with a weak temperature dependence. In contrast, the more appropriate fit using Eq. (2) demonstrates that the true Gilbert damping parameter (red circles) is significantly lower, and the inhomogeneous contribution (due to mosaicity, black squares) is negligible. Instead, there is a finite, temperature-independent TMS contribution (green stars) to the FMR linewidth of $\Gamma = 0.55(5)\,\mathrm{GHz}$. The temperature independence of Γ indicates a structural origin, as discussed in Ref. [15]; therefore, this sample was subject to an in-depth structural and compositional analysis using STEM, which will be compared with the thickest sample of the Al/Py/Al/sapphire series in the following; the 14.7 nm sample was already discussed in detail in Ref. [15].

Figure 4 summarizes the STEM analysis of the Al/Py/Al/sapphire samples with Py thicknesses of (a) 37.1 nm

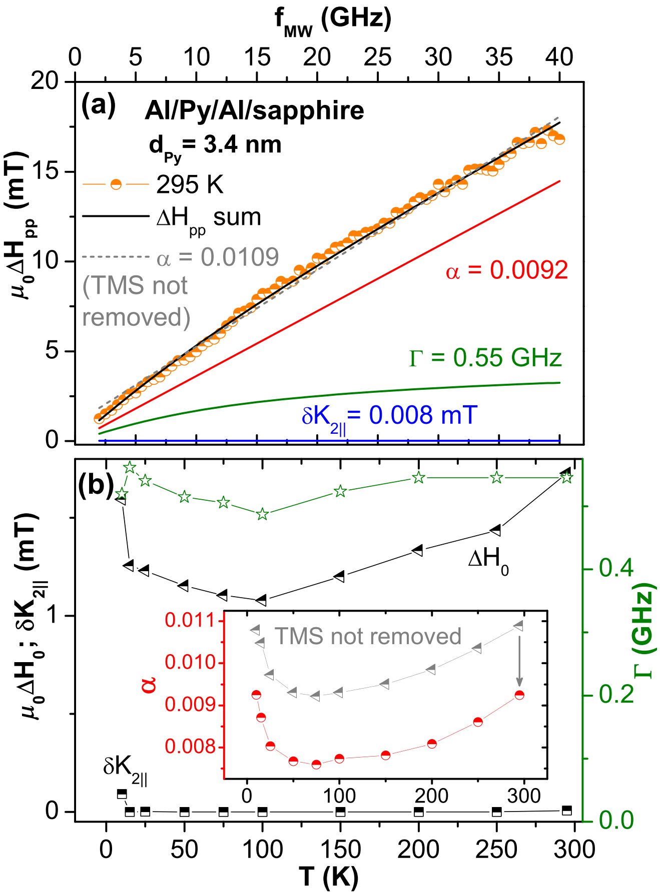

FIG. 3. (a) Frequency dependence of the fitted linewidth $\Delta H_{pp}(f_{MW})$ of the thinnest Al/Py/Al/sapphire with a Py thickness of 3.4 nm recoded at 295 K (orange circles). The black solid line is a fit including different contributions to the FMR linewidth; the gray dashed line is a fit only considering homogeneous and inhomogeneous broadening, see text. (b) Inhomogeneous broadening ΔH_0 (black triangles) as a function of temperature in comparison with the contribution to the FMR linewidth from mosaicity (black squares) and TMS (green stars); the inset shows the reduction of the $\alpha(T)$ behavior upon subtracting the TMS contribution; see text for details.

and (b) 3.4 nm. In addition to some remaining diffraction contrast, the HAADF-STEM images in Fig. 4 are dominated by atomic-number contrast. Therefore, the Py film can be easily distinguished from the Al cap and sapphire substrate. EDXS-based spectrum imaging analysis of the marked region results in the element distribution maps of O, Al, Fe, and Ni, and the corresponding elemental line profile intensities are computed as described in more detail in Ref. [15]. Figure 4 only shows the superimposed O/Al and Ni/Fe maps, which allow us to separate the Py film from the (partially oxidized) Al cap and the Al spacer from the substrate. Because after TEM specimen preparation the lamella was briefly exposed to ambient conditions, its side walls became slightly oxidized, which explains the finite oxygen signal across the Py film. Note that the slightly tilted plateau of the profiles, especially visible for the thick Py film in Fig. 4(a), indicates that the side walls of the TEM lamella are not perfectly parallel. Rather, the TEM lamella is slightly thicker toward the substrate.

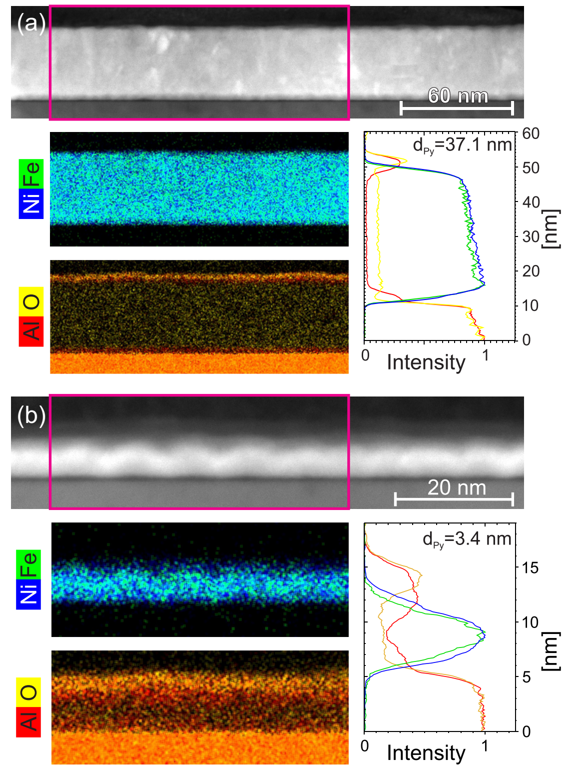

FIG. 4. HAADF-STEM images of the Al/Py/Al/sapphire samples with Py thicknesses of (a) 37.1 nm and (b) 3.4 nm and overlay of the corresponding element distribution maps of Fe/Ni and Al/O together with the extracted line-intensity profiles for all elements. The regions of the element analyses are marked by purple boxes; note the different scale bars in (a) and (b).

The thickest Py film of the Al/Py/Al/sapphire series presented in Fig. 4(a) shows a rather homogeneous appearance of the Py film with well-defined interfaces. Toward the Al spacer, Al is visible without the presence of oxygen, and the transition to Ni/Fe appears rather abrupt, although it is known that the Al spacer layer grows in an islandlike mode [15]. The interface to the Al cap is less abrupt, mostly due to the polycrystalline growth of the Py layer, which results in a slightly wavy surface. The Al cap itself is oxidized from the top, but Py is prevented from oxidation. In contrast, the 3.4 nm Py film in Fig. 4(b) clearly has a wavy appearance in the HAADF-STEM image. The interfaces are both less defined, and in the intensity profiles, Al is found almost across the entire Py film range; however, this is mostly due to the islandlike growth of the Al spacer and not due to chemical intermixing on the atomic scale. These observations have been made for four different regions of the TEM lamella; therefore, Fig. 4(b) is representative for the entire sample. In contrast, the 3.4 nm Py film without an Al spacer layer has a well-defined, abrupt interface to the sapphire, and the Py film itself appears smooth without any similar waviness (not shown). Therefore, the waviness of the 3.4 nm Py film with an Al spacer can readily explain the temperature-independent TMS contribution to the FMR linewidth, as seen in Fig. 3; its magnitude of only 0.5 GHz is smaller than the TMS contribution of 2.4 GHz for the 14.7 nm Py film with a thicker

Al spacer in Ref. [15]. Obviously, this thin sample is right at the border of developing a sizable TMS contribution, which is already absent for the 4.7-nm-thick Py shown in Fig. 2(c). It may also contribute to the more pronounced reduction of M_s seen in Fig. 1(c) via slightly increased chemical intermixing visible in the two-dimensional (2D) element distribution maps. This also leads to a larger uncertainty in deriving the proper net thickness of the Py since, for this film, the two wavy interfaces dominate across the largest part of the thickness, while the structurally undisturbed inner part is relatively narrow. This has been verified by a comparable TEM analysis conducted on the 4.7 nm pair of samples where the fraction of the film being not wavy is clearly increased (not shown), which coincides with the absence of any evident TMS contribution for the sample with an Al spacer. However, in the Al/Py/sapphire sample series, a different kind of TMS contribution is found which was already briefly mentioned in Ref. [14].

Figure 5 shows the peak-to-peak FMR linewidth ΔH_{pp} as a function of microwave frequency f_{MW} for the thinnest Al/Py/sapphire sample at (a) 295 K and (b) 15 K. At 295 K, there is no obvious deviation from a purely linear Gilbert-like behavior of the magnetic damping. Consequently, the FMR linewidth can be fitted best without a TMS contribution, a negligible mosaicity of $K_{2\parallel}$, and a Gilbert α of 0.0101. In contrast, at 15 K, there is a visible deviation from the linear behavior, and accordingly, the best fit yields a TMS contribution of $\Gamma = 1.53$ GHz, a small mosaicity contribution, and $\alpha = 0.0095$. However, if the TMS contribution is forced to be zero, this results in an apparent increase of α to about 0.014, which is similar to the sample with an Al spacer in Fig. 3. The TMS contribution in the sample series without an Al spacer is obviously temperature dependent, and its size has been fitted for the entire thickness series at all temperatures. Figure 5(c) exemplarily shows α as a function of the inverse Py thickness at 295 K (orange squares) and 15 K (blue pentagons), where for the latter, the TMS contribution has been fitted separately as well as ignoring the TMS contribution at 15 K and only fitting a Gilbert-like behavior (gray triangles). Both datasets are linear in $1/d$, indicating bulk and interface contributions; however, while the bulk contribution is identical within experimental error, the interface contribution is halved. In turn, the artificially increased α, for cases where the TMS contribution is disregarded (or experimentally overlooked due to a too narrow available frequency range of the instrument), becomes less severe the thicker the Py film is. Note that the second gray triangle from the left corresponds to the 14.7 nm sample which hase already been discussed in our previous work [15]. The changes in α with and without correcting for the TMS are small but still visible. It is therefore obvious that one must fit the TMS contribution separately to obtain the pure Gilbert damping parameter α.

Summarizing this part, in the two sample series, two different kinds of TMS contributions have been identified: (i) In the Al/Py/Al/sapphire series, the increased waviness of the thinnest Py film (3.4 nm) leads to a small, temperature-independent TMS contribution; all other samples behave purely Gilbert-like; and (ii) in the Al/Py/sapphire series, all samples have a temperature-dependent TMS contribution, which is zero at elevated temperatures but increases at low temperatures; it is most prominent for the thinnest sample. The latter contribution will be briefly discussed in the following.

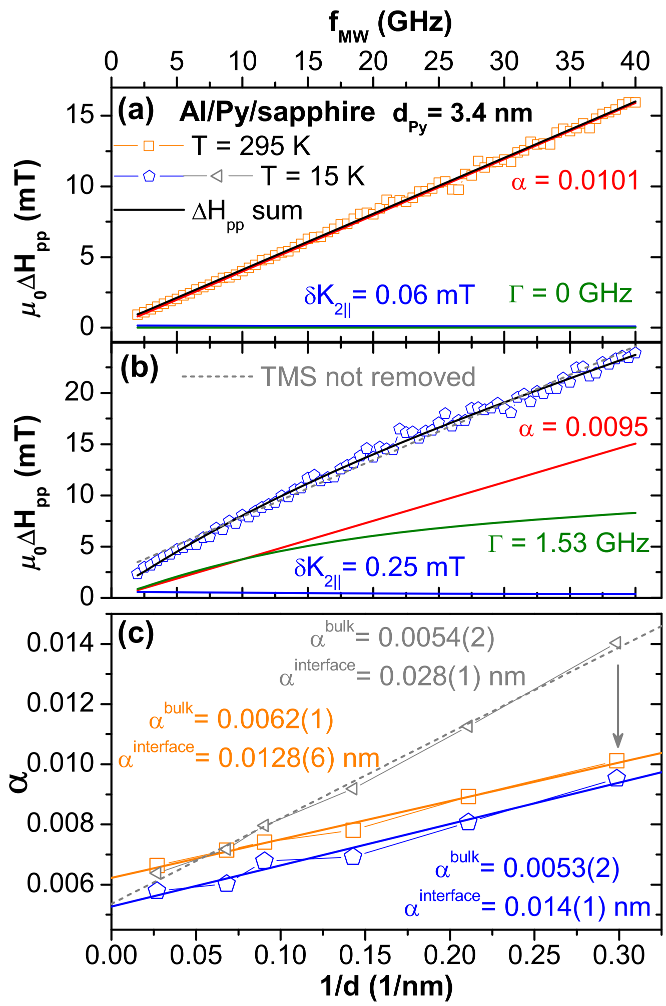

FIG. 5. Frequency dependence of the fitted linewidth $\Delta H_{pp}(f_{MW})$ of Al/Py/sapphire with a Py thickness of 3.4 nm recorded at (a) 295 K (orange squares) and (b) 15 K (violet pentagons). The black solid lines are fits including different contributions to the FMR linewidth; in (b), the gray dashed line is a fit only considering homogeneous and inhomogeneous broadening, see text. (c) Resulting dependence of the fitted α at 295 K (orange squares) and 15 K (blue pentagons) vs inverse Py thickness; the resulting bulk and interface contributions are provided. Gray triangles show the 15 K $\alpha(1/d)$ data without removing the TMS contribution, see text.

C. Bulk and interface contributions to the damping

The inset of Fig. 6(a) shows the fitted TMS contribution Γ as a function of the inverse Py thickness at 295 K (orange squares) and 15 K (blue pentagons) for the entire Al/Py/sapphire series. While there is no sizable TMS contribution at 295 K, a clear TMS contribution is seen at 15 K which is linear in $1/d$, suggesting that it can be split into bulk and interface contributions according to Eq. (5). A linear fit yields a negligible bulk contribution, i.e., the TMS contribution is an interfacial effect. Comparable fits have been made

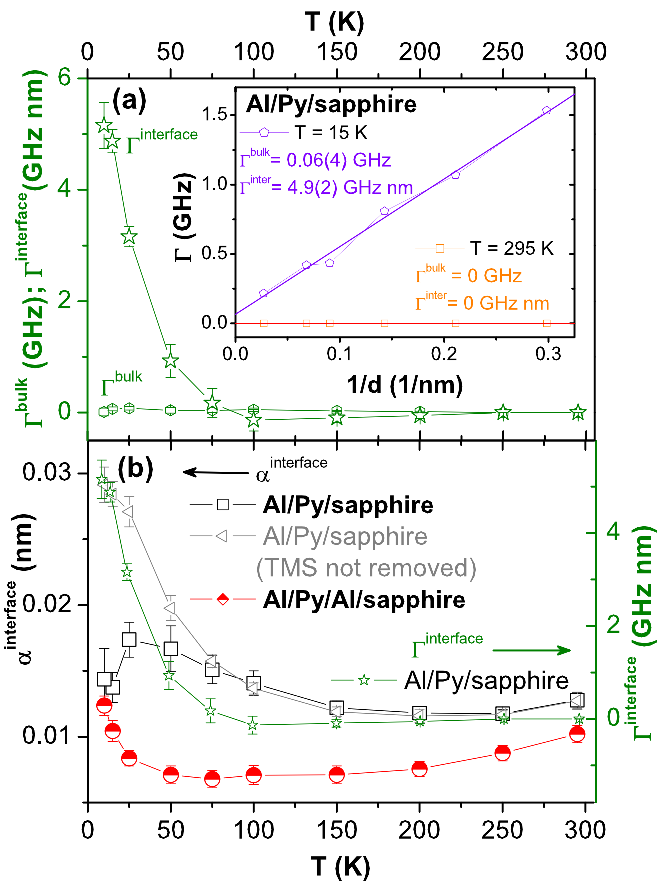

FIG. 6. The inset of (a) shows the TMS contribution of the entire Al/Py/sapphire sample series as a function of inverse Py thickness at 15 K (violet pentagons) and 295 K (orange squares). (a) shows the resulting full temperature dependence of the interface (green stars) and bulk (green squares) contributions to the TMS parameter Γ. (b) Full temperature dependence of the interfacial contribution $\alpha^{\text{interface}}$ of the Al/Py/Al/sapphire (red circles) and Al/Py/sapphire (black squares) sample series after removing the TMS contribution to the FMR linewidth. In addition, the interfacial TMS contribution $\Gamma^{\text{interface}}$ (green stars) is compared with the inhomogeneous broadening without TMS removal (gray triangles).

for all temperatures, and Fig. 6(a) compiles the temperature dependence of the bulk (green squares) and interface (green stars) contributions of Γ as a function of temperature. The bulk contribution is negligible at all temperatures, while a sizable interface contribution starts to set in below 100 K, and it steeply increases down to 10 K. Note that, at 10 K, especially for the thinner samples, the signal-to-noise ratio of the FMR spectra becomes rather low (due to the overall increased linewidth for these samples) so that, for the lowest temperature, the quality of the fit and the linear behavior in $1/d$ are not as good, which results in a larger uncertainty of the fitted parameters, particularly for the interface contribution. The microscopic origin of this interfacial TMS contribution has already been discussed in terms of Py being in contact with the oxidic substrate [14], leading to a potential slight oxidation of Py. However, attempts to verify this hypothesis in the course of the detailed TEM investigation failed so far, mostly due to the sidewall oxidation of the TEM lamella during transfer, which makes it difficult to identify additional oxygen right at the interface next to the oxidic substrate. Nonetheless, the temperature dependence of the interfacial contribution to Γ may be useful for authors of further studies to unambiguously identify the microscopic origin of the (unwanted) TMS contribution. At present, it can only be stated that it can be efficiently suppressed by a thin Al spacer on the expense of potential waviness, resulting again in TMS contributions in cases where the Py layer is very thin, see Fig. 5, or if the Al spacer is too thick, see Ref. [15].

Figure 6(b) compiles the full temperature dependence of the interfacial contribution to the Gilbert-like damping $\alpha^{\text{interface}}(T)$. This has been derived from the slope of the $\alpha(1/d)$ dependencies, as shown in Fig. 5(c) for the Al/Py/sapphire thickness series [yielding the open black squares in Fig. 6(b)] as well as the Al/Py/Al/sapphire series shown in Fig. 7(a) [yielding the half-full red circles in Fig. 6(b)]. Here, the TMS contribution has been subtracted from the overall FMR linewidth. For comparison, the apparent interfacial contribution for the Al/Py/sapphire series without removing the TMS contribution is shown (open triangles), which can be compared with the interfacial contribution of the TMS $\Gamma^{\text{interface}}$ (green stars), which has been scaled to fit the uncorrected $\alpha^{\text{interface}}$. It can be nicely seen that the functional behavior of both is rather similar, which in turn suggests that the Gilbert-like interfacial contribution is, within the error margins, temperature independent. However, it should be noted that the separation of the two components $\alpha^{\text{interface}}$ and $\Gamma^{\text{interface}}(T)$ from a single set of data leads to an increased uncertainty of the derived values so that the apparent maximum of $\alpha^{\text{interface}}(T)$ around 25–50 K is experimentally not significant. Despite these limitations, the overall $\alpha^{\text{interface}}(T)$ for the Al/Py/sapphire series is higher for all temperatures than the Al/Py/Al/sapphire series, i.e., the presence of an Py/sapphire interface is disadvantageous in two ways: It leads to an additional TMS contributions at low temperatures, and in addition, it increases the pure Gilbert-like interfacial contribution to the overall damping. In contrast, the presence of two Py/Al interfaces, i.e., the Al/Py/Al/sapphire series, underlines that this interface allows a low interfacial contribution to the overall damping, which is initially decreasing with temperature with a minimum around 75 K, below which it slightly increases again. Note that, if one considers the two Al/Py interfaces as equivalent, one could even separate the contributions of a single Al/Py interface by halving the $\alpha^{\text{interface}}(T)$ contribution of the Al/Py/Al/sapphire series. Likewise, the Py/sapphire interface is derived by subtracting the halved contribution from $\alpha^{\text{interface}}(T)$ from the Al/Py/sapphire series. This leaves the overall temperature dependence unchanged but makes the local maximum for the Py/sapphire interface more pronounced; however, the detailed XRR and TEM analysis is not very supportive of two equivalent Al/Py interfaces because the waviness of the two interfaces is not identical, see also the in-depth analysis in Ref. [15].

Figure 7(a) exemplarily shows the $\alpha(1/d)$ dependence for the Al/Py/Al/sapphire series at 295 K (half orange circles) and 10 K (half violet pentagons). In addition, for the thinnest sample of 3.4 nm thickness, α is shown without subtracting the TMS contribution (half triangles), see also Fig. 3(a). It is clearly visible that, without subtracting the TMS contribution,

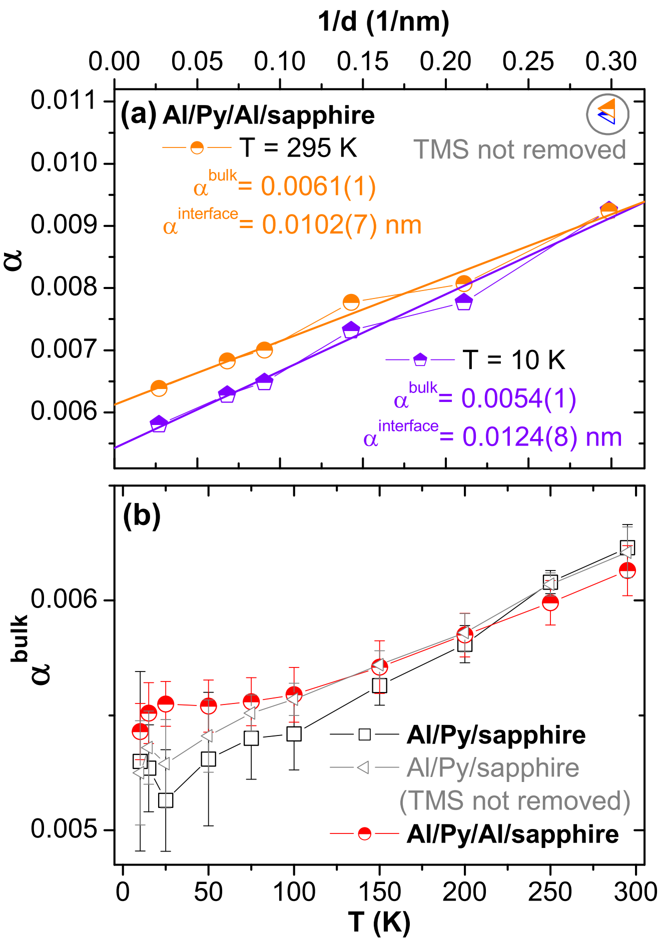

FIG. 7. (a) Dependence of α of the entire Al/Py/Al/sapphire sample series as a function of inverse Py thickness at 295 K (orange circles) and 10 K (violet pentagons) together with the resulting bulk and interface contributions to the Gilbert damping. The triangles marked by a gray circle indicate the α for the thinnest sample when the TMS contribution is not subtracted. (b) Full temperature dependence of the bulk contribution α^{bulk} of the Al/Py/Al/sapphire (red circles) and Al/Py/sapphire (black squares) sample series after removing all TMS contributions to the FMR linewidth. In addition, the Al/Py/sapphire series is shown without prior removal of the TMS contribution (gray triangles).

the functional behavior of $\alpha(1/d)$ is not linear, whereas after the removal of the TMS contributions, all data points can be nicely fitted by a line. It is noteworthy that, if the data are not corrected for the TMS contribution, not only the interfacial contribution is artificially increased, but also the resulting bulk contribution is reduced; this should be kept in mind when comparing the results of this work with earlier ones, e.g., in fig. 2(c) of Ref. [16], it is visible that α for the thinnest sample lies higher than derived from the extrapolated linear behavior of the remaining thicker films. Since in Ref. [16] the frequency range was limited to 15 GHz, any kind of similar TMS contribution in this sample may go undetected because the visible deviation for an apparently linear behavior of $\Delta H(f_{\mathrm{MW}})$ can only be seen if the FMR linewidth is studied up to at least 25 GHz, see Fig. 3(a). This may readily explain deviations in the derived numerical values for the interface and particularly the bulk contribution to α.

Finally, Fig. 7(b) compiles the full temperature dependence of bulk contribution to the Gilbert-like damping $\alpha^{\mathrm{bulk}}(T)$ for the Al/Py/sapphire (open black squares) and Al/Py/Al/sapphire (half red circles) thickness series. Again, for comparison, also the Al/Py/sapphire series is shown without removing the TMS contribution (open gray triangles). As already visible for the data at 15 K in Fig. 5(c), the bulk contributions with and without removing the TMS contributions at lower temperatures are identical within error bars for all temperatures. This underlines the fact that, for this sample series, the TMS contribution is a purely interfacial effect, corroborating the $\Gamma(1/d)$ behavior in Fig. 6(a). In addition, the extracted $\alpha^{\mathrm{bulk}}(T)$ of the Al/Py/Al/sapphire series is, within experimental accuracy, identical to the one of the Al/Py/sapphire series. Therefore, the functional behavior of $\alpha^{\mathrm{bulk}}(T)$ can be taken as the intrinsic property of magnetron-sputtered Py, which is only modified by interfacial contributions due to the adjacent material and/or additional TMS contributions due to wavy interfaces or interfaces to oxidic substrates. This is in some regard remarkable since $\alpha^{\mathrm{bulk}}(T)$ monotonously drops with decreasing temperature and plateaus below 100 K.

IV. DISCUSSION

In a first step, the magnitude of $\alpha^{\mathrm{bulk}}(T)$ shall be discussed. At 295 K, $\alpha^{\mathrm{bulk}} = 0.0061(1)$, while it drops to $\alpha^{\mathrm{bulk}} = 0.0054(1)$ at 10 K. These values are larger than the findings in Ref. [16], where $\alpha^{\mathrm{bulk}}(T)$ is reported to be between 0.0055(5) at 300 K and 0.0048(4) at 10 K; however, these findings may be explained by the experimental limitations of that early study, as discussed above. Nonetheless, the functional behavior, i.e., the monotonic drop with decreasing temperature down to a plateaulike behavior below 100 K, is identical. One can thus consider these two findings to be consistent and thus representative for the bulk contribution of sputtered Py thin films, disregarding the different interfacial contributions. Note that we are not aware of any other comparable study where both temperature and thickness dependence have been studied by broadband FMR for Py thin films.

In a second step, the functional behavior of $\alpha^{\mathrm{bulk}}(T)$ shall be discussed. It closely resembles a resistivitylike behavior which has been associated with electronic interband scattering processes, see, e.g., the discussion in Ref. [11]. In that work, epitaxial (uncapped) Fe films on different substrates but at fixed Fe thickness have been investigated, and both conductivitylike and resistivitylike contributions have been found. In the present case, in contrast with Ref. [11] but in agreement with Ref. [16], no conductivitylike behavior can be observed for α^{bulk} in sputtered Py, suggesting the absence of intraband scattering events. However, the separate modeling of the interband processes in Ref. [10] suggests a monotonically decreasing contribution, while the experimental data exhibit a plateaulike behavior. Therefore, the conductivitylike/intraband mechanism can only be taken as small compared with the resistivitylike/interband processes in polycrystalline Py film in comparison with the crystalline sample studied, e.g., in Ref. [11]. A clear conductivitylike contribution, i.e., an increase toward low temperatures, is only seen in the interfacial contribution, where $\alpha^{\text{interface}}(T)$ increases at low temperatures, forming a local minimum in $\alpha^{\text{interface}}(T)$, as predicted by the combination of both relaxation processes [10]. However, for Al/Py/sapphire, this increase at low T is not necessarily due to intraband scattering mechanisms since this interfacial contribution is dominated by the TMS contribution which is not due to electronic but magnonic scattering events. Only in the Al/Py/Al/sapphire series may a small conductivitylike contribution be seen. However, compared with the temperature variation of the resistivitylike contribution, it is much less pronounced than reported for the Fe films in Ref. [11], where this contribution gives rise to the largest variation of α with temperature. In turn, the result in Fig. 7(b) supports theoretical predictions that, in pure metals (realized here as bulk contribution of a polycrystalline Py film), intraband scattering, i.e., conductivitylike damping is absent [21]. Alternatively, the influence of polycrystallinity of the Py films in the present case may lead to a rather efficient suppression of the intraband/breathing Fermi surface/conductivitylike contribution compared with crystalline samples. Apparently, the separation in terms of bulk and interface contributions to the Gilbert-like damping for polycrystalline films in the present study as well as in Ref. [16] suggests that we reconsider the underlying microscopic mechanisms for modeling the magnetic damping in terms of the bulk vs interfacial character of conductivitylike vs resistivitylike contributions to the magnetic damping as a function of temperature. In addition, a refined modeling of the interfacial TMS contributions is needed to account for the two rather different behaviors in terms of temperature dependence, as shown in Fig. 3(b) for the wavy interface and Fig. 6(a) for the contact with an oxidic substrate, denoted by the green stars, respectively.

V. SUMMARY

The magnetic damping in Al/Py/sapphire and Al/Py/Al /sapphire sample series was systematically investigated as a function of Py layer thickness using broadband FMR in the temperature range between 10 and 295 K. The full set of data allows us to separate the Gilbert-like damping α from contributions of TMS processes to the FMR linewidth. Further, both contributions could be separated into bulk and interface contributions and their respective temperature dependencies. Two kinds of TMS contributions have been identified: (i) a temperature-independent TMS contribution induced for the 3.4-nm-thick Py film of the Al/Py/Al/sapphire series having a wavy appearance induced by the islandlike growth of the Al spacer layer, as observed before in thicker Py layers on thicker Al spacer layers [15], and (ii) a TMS contribution of purely interfacial character in the Al/Py/sapphire series induced by the direct contact of Py with the oxidic substrate, which is absent above 50 K and increases at lower temperatures; such a contribution has been reported before for several Py films in proximity to different kinds of oxidic layers [14]. Once these TMS contributions are removed from the FMR linewidth, the remaining Gilbert-like damping can be separated into bulk and interface contributions and their respective temperature dependencies. While the Al/Py/sapphire interfaces result in a slightly increased interface contribution with no significant temperature dependence, the Al/Py/Al interfaces exhibit an interfacial contribution which is smaller at all temperatures and shows a local minimum at 75 K with a slight increase below as well as above 75 K, being indicative of both conductivitylike and resistivitylike behavior. In contrast, the bulk contribution $\alpha^{\text{bulk}}(T)$ is virtually identical for both sample series, and no increase at low temperatures can be observed, i.e., the bulk contribution of α of Py is only of resistivitylike character. Here, $\alpha^{\text{bulk}}(T)$ for sputtered Py ranges from 0.0061(1) at 295 K down to 0.0054(1) at 10 K. Since all other contributions from interfaces including TMS processes have been considered separately, these findings can be taken as the intrinsic magnetic damping of sputtered Py thin films.

ACKNOWLEDGMENTS

The authors acknowledge Annette Kunz for TEM specimen preparation. Furthermore, the use of the HZDR Ion Beam Center TEM facilities and the funding of TEM Talos by the German Federal Ministry of Education and Research (Grant No. 03SF0451) in the framework of HEMCP are acknowledged.

DATA AVAILABILITY

The data that support the findings of this article are not publicly available. The data are available from the authors upon reasonable request.

[1] L. Landau and E. Lifshitz, On the theory of the dispersion of magnetic permeability in ferromagnetic bodies, in *Perspectives in Theoretical Physics* (Pergamon, Amsterdam, 1992), Chap. 3, pp. 51–65.

[2] T. L. Gilbert, A phenomenological theory of damping in ferromagnetic materials, IEEE Trans. Magn. **40**, 3443 (2004).

[3] B. Heinrich, R. Urban, and G. Woltersdorf, Magnetic relaxation in metallic films: Single and multilayer structures, J. Appl. Phys. **91**, 7523 (2002).

[4] M. A. W. Schoen, J. M. Shaw, H. T. Nembach, M. Weiler, and T. J. Silva, Radiative damping in waveguide-based ferromagnetic resonance measured via analysis of perpendicular standing spin waves in sputtered Permalloy films, Phys. Rev. B **92**, 184417 (2015).

[5] S. Wu, D. A. Smith, P. Nakarmi, A. Rai, M. Clavel, M. K. Hudait, J. Zhao, F. M. Michel, C. Mewes, T. Mewes, *et al.*, Room-temperature intrinsic and extrinsic damping in polycrystalline Fe thin films, Phys. Rev. B **105**, 174408 (2022).

[6] Y. Tserkovnyak, A. Brataas, and G. E. W. Bauer, Enhanced Gilbert damping in thin ferromagnetic films, Phys. Rev. Lett. **88**, 117601 (2002).

[7] B. Heinrich, *Spin Relaxation in Magnetic Metallic Layers and Multilayers* (Springer, New York, 2004), Vol. III.

[8] V. Kambersky, On ferromagnetic resonance damping in metals, Czech. J. Phys. **26**, 1366 (1976).

[9] V. Kambersky, On the Landau-Lifshitz relaxation in ferromagnetic metals, Can. J. Phys. **48**, 2906 (1970).

[10] K. Gilmore, M. D. Stiles, J. Seib, D. Steiauf, and M. Fähnle, Anisotropic damping of the magnetization dynamics in Ni, Co, and Fe, Phys. Rev. B **81**, 174414 (2010).

[11] B. Khodadadi, A. Rai, A. Sapkota, A. Srivastava, B. Nepal, Y. Lim, D. A. Smith, C. Mewes, S. Budhathoki, A. J. Hauser, *et al.*, Conductivitylike Gilbert damping due to intraband scattering in epitaxial iron, Phys. Rev. Lett. **124**, 157201 (2020).

[12] J. Lindner, K. Lenz, E. Kosubek, K. Baberschke, D. Spoddig, R. Meckenstock, J. Pelzl, Z. Frait, and D. L. Mills, Non-Gilbert-type damping of the magnetic relaxation in ultrathin ferromagnets: Importance of magnon-magnon scattering, Phys. Rev. B **68**, 060102(R) (2003).

[13] R. D. McMichael and P. Krivosik, Classical model of extrinsic ferromagnetic resonance linewidth in ultrathin films, IEEE Trans. Magn. **40**, 2 (2004).

[14] V. Ney, R. Salikhov, K. Lenz, O. Hellwig, J. Lindner, and A. Ney, Influence of oxidic and metallic interfaces on the magnetic damping of Permalloy thin films, Phys. Rev. Mater. **7**, 124403 (2023).

[15] V. Ney, K. Lenz, F. Ganss, R. Hübner, J. Lindner, and A. Ney, Influence of interface morphology on the magnetic damping of Al-sandwiched Permalloy thin films, Phys. Rev. Mater. **8**, 114410 (2024).

[16] Y. Zhao, Q. Song, S.-H. Yang, T. Su, W. Yuan, S. S. P. Parkin, J. Shi, and W. Han, Experimental investigation of temperature-dependent Gilbert damping in Permalloy thin films, Sci. Rep. **6**, 22890 (2016).

[17] M. Buchner, K. Höfler, B. Henne, V. Ney, and A. Ney, Tutorial: Basic principles, limits of detection, and pitfalls of highly sensitive SQUID magnetometry for nanomagnetism and spintronics, J. Appl. Phys. **124**, 161101 (2018).

[18] J. O. Rantschler, B. B. Maranville, J. J. Mallett, P. Chen, R. D. McMichael, and W. F. Egelhoff, Jr., Damping at normal metal/Permalloy interfaces, IEEE Trans. Magn. **41**, 3523 (2005).

[19] Y. Liu, Z. Yuan, R. J. H. Wesselink, A. A. Starikov, and P. J. Kelly, Interface enhancement of Gilbert damping from first principles, Phys. Rev. Lett. **113**, 207202 (2014).

[20] The bulk contribution of $\mu_0 M_s = 0.99(2)\,\mathrm{T}$ derived by SQUID is in satisfying agreement with $\mu_0 M_{\mathrm{eff}} = 1.07(1)\,\mathrm{T}$ derived by Cryo-FMR, whereby the uncertainty only refers to the linear regression of the $1/d$-analysis not considering the uncertainties of the individual values of M_s and M_{eff}, respectively.

[21] D. M. Edwards, The absence of intraband scattering in a consistent theory of Gilbert damping in pure metallic ferromagnets, J. Phys.: Condens. Matter **28**, 086004 (2016).